Available online at www.sciencedirect.com
ScienceDirect
Journal of Power Sources 170 (2007) 334–344
JOURNAL OF POWER SOURCES
www.elsevier.com/locate/jpowsour

Experimental investigation of liquid water formation and transport in a transparent single-serpentine PEM fuel cell

Dusan Spernjak, Ajay K. Prasad, Suresh G. Advani *

Fuel Cell Research Laboratory, Department of Mechanical Engineering, 126 Spencer Laboratory, University of Delaware, Newark, DE 19716, USA

Received 26 January 2007; received in revised form 30 March 2007; accepted 3 April 2007
Available online 18 April 2007

Abstract

Liquid water formation and transport were investigated by direct experimental visualization in an operational transparent single-serpentine PEM fuel cell. We examined the effectiveness of various gas diffusion layer (GDL) materials in removing water away from the cathode and through the flow field over a range of operating conditions. Complete polarization curves as well as time evolution studies after step changes in current draw were obtained with simultaneous liquid water visualization within the transparent cell. The level of cathode flow field flooding, under the same operating conditions and cell current, was recognized as a criterion for the water removal capacity of the GDL materials. When compared at the same current density (i.e. water production rate), higher amount of liquid water in the cathode channel indicated that water had been efficiently removed from the catalyst layer.

Visualization of the anode channel was used to investigate the influence of the microporous layer (MPL) on water transport. No liquid water was observed in the anode flow field unless cathode GDLs had an MPL. MPL on the cathode side creates a pressure barrier for water produced at the catalyst layer. Water is pushed across the membrane to the anode side, resulting in anode flow field flooding close to the H_2 exit.

Keywords: PEM fuel cell; Liquid water transport; Visualization; Gas diffusion layer; Microporous layer

1. Introduction

Humidification has to be carefully optimized in polymer electrolyte membrane fuel cells (PEMFC). Extremes in humidity levels at both the low end (membrane dehydration) and the high end (cathode flooding) of the range can significantly reduce PEMFC performance. Due to these conflicting requirements, the window for operating conditions for a PEMFC is very narrow. The cell is usually operated at the flooding limit, and some areas of the catalyst layer can be covered by condensing water. Since flooding has been identified as one of the main current-limiting processes, understanding and optimizing liquid water transport throughout the cell is critical to improving PEMFC performance. Moreover, flooding can also take place at lower current densities, if the gas flow rate and/or temperature (i.e. equilibrium vapor pressure) are low [1–3].

Various experimental techniques have been employed to investigate water dynamics in PEMFC. Membrane dehydration is commonly observed through the increase in the cell (i.e. membrane) resistance [1,6]. To detect cathode flooding, one can use *global* tools such as fully saturated air at the exit [1] and increase in the pressure drop [3,6,7]. Flooding is also associated with a drop in the cell output power. *Local* information about the flooded regions in the cell can be obtained by current and temperature distribution measurements [8]. Besides aforementioned physical indicators of flooding (current, temperature, pressure drop, and relative humidity), various *imaging techniques* can be used to investigate two-phase dynamics inside the cell. Known possibilities are direct flow visualization [7–10], neutron radiography [11], and magnetic resonance imaging [12].

Although direct flow visualization requires a special cell design (Fig. 1), it is a very attractive experimental technique since optical access to the channels provides high spatial and/or temporal resolution, depending on the combination of optics and recording equipment. Direct visualization offers the advantage of investigating two-phase phenomena at different length

* Corresponding author. Tel.: +1 302 831 8975; fax: +1 302 831 3619.
E-mail addresses: spernjak@udel.edu (D. Spernjak), prasad@udel.edu (A.K. Prasad), advani@udel.edu (S.G. Advani).

0378-7753/$ – see front matter © 2007 Elsevier B.V. All rights reserved.
doi:10.1016/j.jpowsour.2007.04.020

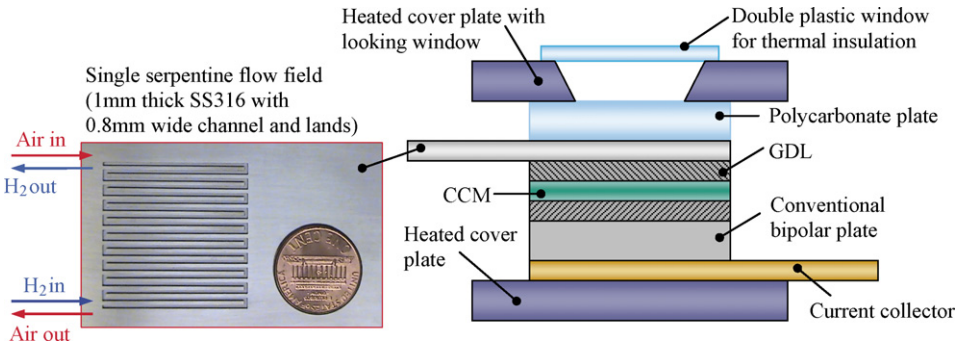

Fig. 1. Operational transparent PEMFC.

scales in an operating PEMFC environment, ranging from the cell/channel level [7,8], to the smaller scale level of the GDL pore/droplet [9,10], and down to the micro-scale level of water dynamics on the catalyst layer surface (recent work in our laboratory). Complete cathode flow fields with parallel channels were visualized in [7,8], with fields of view 6.5 mm × 62 mm, and 45 mm × 45 mm, respectively. Liquid water buildup was correlated with the increase in the pressure drop, while complete channel blockage was identified as the cause of the sharp prolonged decrease in current density at fixed voltage [7]. In addition, Tüber et al. [7] investigated the influence of the wetting property of the GDL on the cell performance and flooding, by modifying the standard Toray carbon paper TGP-H-90 to be strongly hydrophobic (20 wt.% PTFE) or hydrophilic. Optical imaging in [8] was used to provide complementary information about temperature and current distribution measurements. When water is in the vapor phase, higher temperature regions correspond to higher currents. Condensed water changes this correlation by lowering the current density in flooded areas, accompanied by local increase in temperature, attributed to the release of latent heat of condensation. Since the cells in [7,8] were not heated externally (ambient operating temperature and pressure), the investigation was limited to very low current densities (i.e. water production rates). Performance comparable to conventional cells, at higher operating temperatures of 70 and 80 °C, and 2 atm abs pressure, was reported in [9,10]. Wet-proofed Toray carbon paper TGP-H-90 (20 wt.% PTFE) with a microporous layer (MPL) was used as the GDL. Small portions of the parallel cathode flow field were visualized in order to investigate the droplet formation at the GDL/channel interface, followed by the droplet interactions with the channel walls. While such a small field of view (of the order of only a few millimeters) does not allow one to estimate the overall level of the flow field flooding, it enables one to observe micro-scale phenomena, such as repeatable droplet growth as water is wicked from the GDL through preferential openings at the GDL surface in the flow channel [9,10].

The visualization technique provides mainly qualitative data, as the top view of the channel typically does not offer depth perception. Since the thickness of water films, slugs and droplets often cannot be evaluated, it is very difficult (if not impossible) to quantitatively estimate the amount (volume) of water in the channels. Second, the transparency of water, coupled with highly reflective background comprised of GDL carbon fibers, represent obstacles for image processing. Estimation of the water volume has been achieved only at high magnification [9,10], and has been limited to the case when discrete droplets grow on the surface of the hydrophobic GDL. Droplet detachment diameter has been correlated with the mean gas velocity in the channel [10]. In spite of its qualitative nature, visualization has helped in understanding the influence of water dynamics on the cell performance.

The present work examines the two-phase flow inside a single-serpentine PEMFC by direct experimental visualization. Our approach is to correlate the overall flow field flooding and the cell performance, similar to the entire-cell visualization [7,8] of the parallel channels. While studies [7,8] were done at ambient temperature and low current densities (maximum around 0.25 A cm^{-2}), the present study investigates the flooding phenomena under realistic operating conditions at high water production rates (up to almost order of magnitude higher), with cell performance comparable to conventional cells. Second, previous studies used Toray TGP-H carbon paper: either standard [7,8] or modified in-house [7,9,10]. While Hakenjos et al. [8], Yang et al. [9], and Zhang et al. [10] did not investigate the influence of the GDL material, Tüber et al. [7] reported visualization results for GDLs with different wetting properties (untreated, hydrophobized, and hydrophilized Toray paper). The present work compares the performance of several commercially available GDL materials from three GDL manufacturers. In addition to Toray carbon paper, wet-proofed non-woven GDLs by SGL Carbon (both with and without the MPL), as well as the woven carbon cloth by Ballard, were tested in the serpentine cell. Our objective was to elucidate the influence of the GDL media on the cell performance through water management. An important distinction from the previous work is the investigation of the MPL influence on water management, through the visualization of the anode channel flooding. Experiments with conventional cells [13] and modeling efforts focusing on two-phase flow through the porous GDL [4,5] indicate that under certain operating conditions flooding may also be anticipated on the anode side, caused by the pressure barrier of the cathode MPL. This effect has not yet been investigated in detail, as the published work has insofar been limited to the visualization of the cathode side. The present study attempts to elucidate the water dynamics across the entire cell, by performing two series of visualization experiments, in

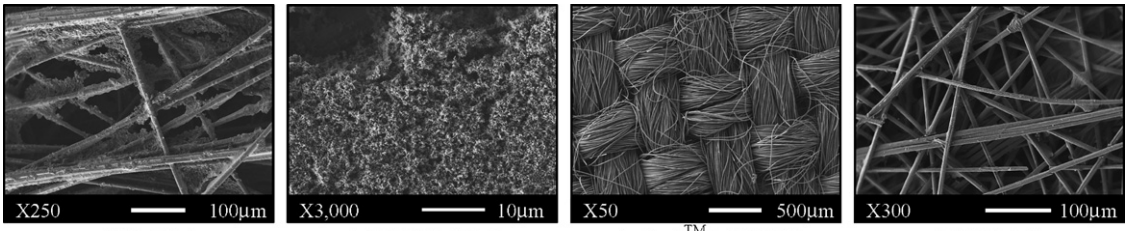

Fig. 2. SEM images of GDL microstructure.

which cathode (Sections 3.1 and 3.2) and anode (Section 3.3) sides were visualized.

2. Experimental

To compare the water management effectiveness of GDL materials, several membrane-electrode assemblies (MEAs) were fabricated with the same catalyst coated membrane (CCM) while varying the GDL. The CCM used was a 25 μm thick Nafion®-based membrane with 0.3 mg cm^{-2} Pt loading on each side (Ion Power, Inc.). The GDL materials tested are listed below (Fig. 2):

- Sigracet® SGL31BA by SGL Carbon Group [14,15].
- Sigracet® SGL31BC and SGL35BC (both with MPL) by SGL Carbon Group [14,15].
- AvCarbTM 1071HCB by Ballard® [16].
- TGP-H-060 by Toray Industries, Inc. [17].

MEAs were first tested in a conventional 10 cm^2 PEMFC (by Fuel Cell Technologies), with a single-serpentine channel cut into Poco Durabraze® graphite bipolar plates. The channel was 0.8 mm wide and 1 mm deep, with 0.8 mm wide lands. A 200 W test station, from Arbin Instruments, was used for monitoring and control of flow, pressure, temperature, humidity and electronic load. Humidity of the gas was controlled by the dew point temperature (DPT) in the humidifier. In all tests, DPT of the inlet gases was the same as the cell temperature. To avoid condensation between the test stand and the fuel cell, gas temperature was raised by 10 °C after passing through the humidifier. The tests were conducted at 1 bar backpressure, with constant flow rates (expressed in standard liters per minute). For conversion to stoichiometries, 0.18 slpm of air and 0.076 slpm of hydrogen correspond to 1 A cm^{-2} equivalent flow rate for our 10-cm^2 cell.

Formation and transport of liquid water were observed using an operational, transparent PEMFC (Fig. 1). The transparent cell has a single-serpentine channel cut through a 1 mm thick stainless steel plate, which also serves as the current collector (Fig. 1). Visual access is allowed through a polycarbonate cover plate. The other half of the cell was retained from the aforementioned conventional cell, with the graphite bipolar plate. Standard stainless steel 316 was used for the flow field, and fogging of the polycarbonate plate was mitigated by heating the cell.

Since our goal was to obtain a global estimation of the flow field flooding, magnification was set to show about 60% of the flow field, which is acceptable since no liquid water was commonly observed in the upstream portion. Visualization images show the area of 2 cm × 3.2 cm. Portions of some images are shown enlarged, to better visualize liquid water formation and transport. Flow direction in all cell tests and the corresponding images of the cathode and anode side is as indicated in Fig. 1 (counter-flow). A digital camcorder (Sony DCR-HC42) was used for imaging (1 frame min^{-1}). A high-speed camera Redlake HG-100K (up to 250 frames s^{-1}) was used to estimate the velocities of water droplets.

While there were variations in both cell performance and water distribution, trends were repeatable. Restarting the cell yielded performance that was repeatable to within 10%. Repeating the tests with different MEAs made with the same GDL material showed up to 20% deviation in the cell output, while the trends in performance after voltage steps and the corresponding water dynamics were preserved.

3. Results and discussion

3.1. Influence of operating conditions

Fig. 3 shows the effect of the air flow rate in the conventional cell at 70 °C, with SGL31BA as the GDL. The peak in performance is achieved as the air flow rate was increased to 1.1 slpm (maximum power density of 1.09 W cm^{-2} at current density of 2.6 A cm^{-2}). Further increase of air flow rate resulted in the performance drop, indicating that the membrane dehydration limit had been reached. This was also seen from increased current oscillations at fixed voltage, and confirmed later in the trans-

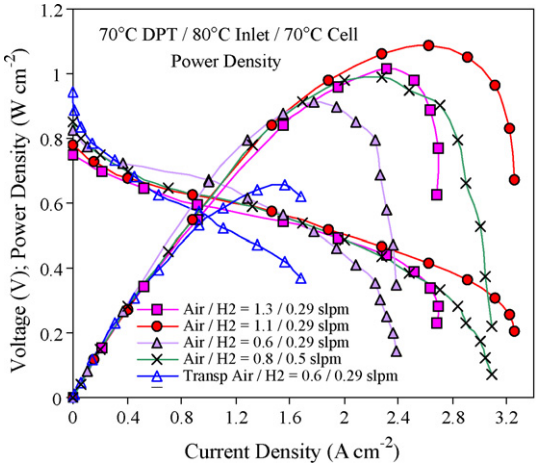

Fig. 3. Influence of flow rates with SGL31BA as GDL.

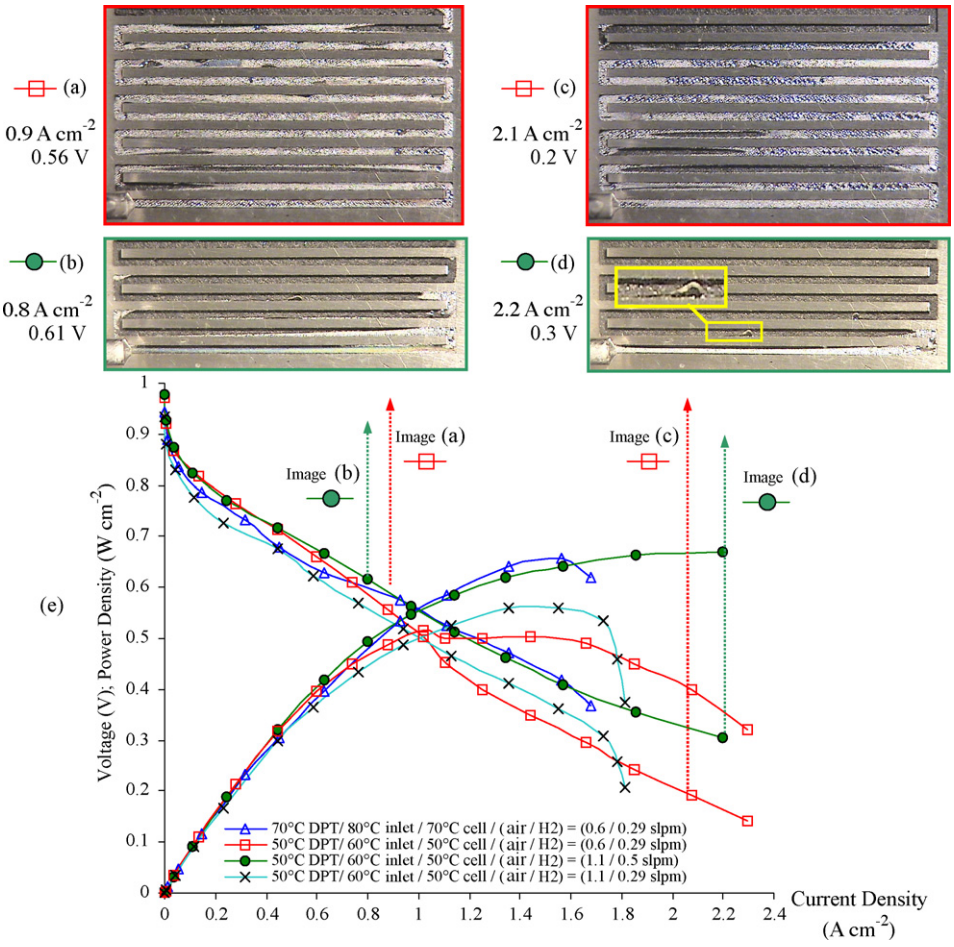

Fig. 4. (a)–(d): Cathode flow field flooding compared at similar current density while recording the polarization curves and (e) performance curves of the transparent cell with SGL31BA at different operating conditions.

parent cell through the absence of liquid water in the cathode channel. Although saturated, the air entering the channel with velocity of 17.1 m s^{-1} showed to have a strong drying effect. An additional curve from the experimental transparent cell is shown for comparison. As expected, the transparent cell performance was lower than the conventional cell, mostly due to lower current collecting and conducting ability of the thin steel plate.

Next, the influence of operating parameters was investigated in the transparent cell, with SGL31BA (5 wt.% PTFE [14,15]) as the GDL (Figs. 4 and 5). The observed origins of liquid water within the cathode channel are as follows:

1. After condensing in the vicinity of the catalyst layer of the cathode side [1,2], liquid water is wicked away through the GDL pores into the channels. For wet-proofed GDL such as SGL materials, discrete droplets emerge periodically at preferential locations on the GDL surface. This periodic nature of water egress at the GDL pore size level has been characterized in [9,10]. While such repeatable water behavior on the GDL surface in the flow channel is caused mainly by the GDL structure, our recent microvisualization of water dynamics on the catalyst layer suggests that it is also promoted by the liquid water accumulation pattern on the underlying catalyst layer surface.
2. Liquid water in the channel may also originate due to the condensation (fogging) on the channel walls, seen as bright white areas on the top channel surface. This is most pronounced after the step increase in the current draw (e.g. when switching from open circuit to 0.4 V), when most of the top channel surface gets instantaneously fogged. Note that no water was observed at open circuit (OCV). Furthermore, no water (be it from the GDL pores or from the condensation on the channel walls), could be seen unless an onset current density was reached. At 50 °C (Fig. 4), occurrence of water was first observed at 0.3 A cm^{-2} for 0.6/0.29 slpm, and at 0.6 A cm^{-2} for 1.1/0.5 slpm of air/H_2. This indicates that although the gas is fully humidified, the occurrence of liquid water in the channel requires oversaturated gas, as reported in [9].
3. Water in the flow field was also observed due to occasional bursts of liquid water from the test stand. This is typically accompanied by instantaneous fogging, similar to the one observed after the step changes in the current draw. Depending on the operating conditions and the GDL used, these bursts can cause drop in the cell performance due to the sudden increase in water content within the cell.

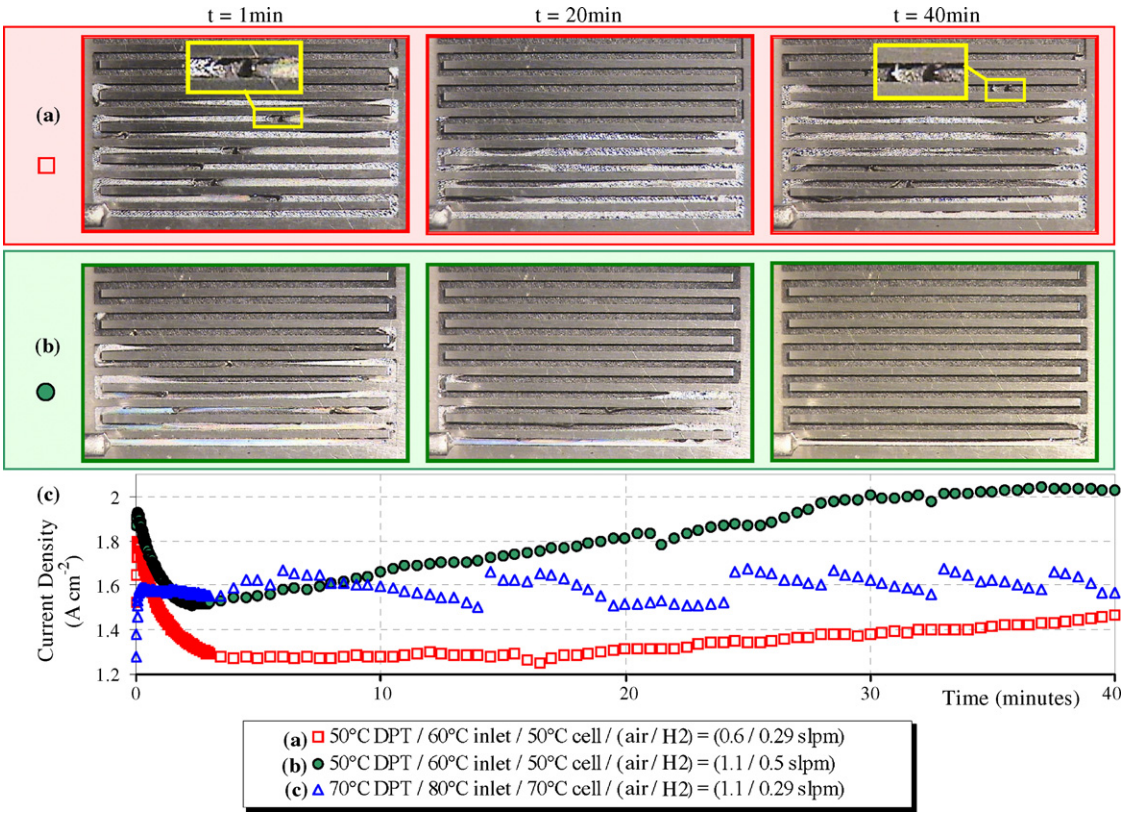

Fig. 5. Time evolution at constant voltage 0.4 V after OCV, with SGL31BA as the GDL at different operating conditions: cell performance (c) with the corresponding cathode flow field images (a) and (b).

Once the liquid water is present in the flow field, several *mechanisms of water transport* within the flow channel were observed. The droplets growing from the GDL pores were readily removed by the gas stream, due to the high inlet air velocity (7.4–16 m s^{-1} for air flow rate of 0.6–1.3 slpm, respectively). At the lower end, 7.4 m s^{-1} and $Re = 726$, the droplet detachment diameter ([10], Eq. (12)) at the serpentine inlet was found to be only 50 μm. In addition, the droplets are often swept away by other droplets, slugs and films that originated from the upstream water accumulation. This mechanism disturbs the periodic pattern, as the droplets emerging from the GDL often do not get the chance to grow and reach their detachment size. When droplets from the GDL come in contact with the (less hydrophobic) channel walls, they either spread into a thin film, or, unless removed, they continue to grow attached to the wall, occupying a large portion of the channel cross section. Such large droplets, of the order of the channel size (as shown in enlarged portion of Fig. 4d), tend to adhere onto the channel wall and progress intermittently along the channel, with typical progression speed of several millimeters per minute. In addition, recording with high-speed camera revealed their recurrent detachment, as the droplets were expelled with velocities as high as 1 m s^{-1}, collecting other droplets along the channel and clearing the fog from the channel walls. Further, previous studies [9,10] reported the flow along the corners (where the sidewalls meet the top channel wall) as a mechanism for water removal. However, corner wetting was not observed in our experiments, as water typically moved along (and cleared) the central portion of the top channel wall, while leaving the edges fogged. This can be explained by the Concus–Finn condition for wetting of the wedge corner via capillary pressure [18]. In a rectangular channel, water will wick into the corner if the contact angle of the walls is less than 45°. Static contact angles (at room temperature) for the materials used in our experimental cell were measured to be 78° for polycarbonate, 72° for SS316, and 76° for the polymer graphite used on a non-transparent side of the cell. Therefore, the Concus–Finn condition was not satisfied on either side of our cell. In contrast, gold coating of the sidewalls (contact angle around 40°), and the hydrophilic anti-fog coating on the polycarbonate, induced the corner wetting in [9,10].

Finally, water accumulation and longer residence times were observed at U-turns (especially at outer corners). This is caused mainly by the velocity distribution of the core gas flow. Particle image velocimetry (PIV) measurements [19] in the U-shaped channel identified the regions of recirculation (outer corners of the U-bend) and flow separation (originating at the inner bend corner, i.e. the land tip). The accompanying effect is that flow field portions around U-turns tend to remain fogged for extended periods. To a lesser extent, water accumulation at U-turns was promoted by the temperature distribution. Due to the absence of active cell cooling, slightly lower temperature may be expected around the edges of the flow field than in the central region.

Images in Fig. 4 depict the influence of flow rates on the cathode flow field flooding, compared at two current densities for the cell at 50 °C. While recording the polarization curves, water first appeared in the bottom portion of the cell once the onset current

was reached. As the cell current draw was increased, the flooded area spread from the bottom towards the inlet. At similar current density (i.e. similar water production rate), the amount of liquid water in the cathode channels was much higher at the lower air flow of 0.6 slpm (Fig. 4(a) and (c)) than at 1.1 slpm (Fig. 4(b) and (d)). Although the performance is very similar at lower current densities for the images shown, the difference in the two-phase transport is substantial (compare the images Fig. 4(a) and (b)). Increasing the cell temperature to 70 °C, while keeping other conditions the same as for images Fig. 4(a) and (c), resulted in a dry cathode flow field. This suggests that the cell was operating close to the membrane dehydration conditions. Similarly, only traces of liquid water were observed for 1.1/0.29 slpm at 50 °C. Increasing the hydrogen flow rate to 0.5 slpm (Fig. 4(b) and (d)) indicates that hydrogen mitigated the membrane drying effect of the air flow.

Next, the cell response was recorded after switching from open circuit (OCV) to a constant voltage 0.4 V (Fig. 5). Step increase in the current draw is accompanied by instantaneous fogging of the channel surface. Immediately after, the fog portions got cleared intermittently as the droplets were swept away by the water films and slugs. (Fig. 5(a): Note the slug 'tails' at 1 min, and the clear streaks along the central portions of the channel at 20 min.) After initial flooding due to the sudden jump in water production rate, the cell operating at higher air flow rate (1.1 slpm air, Fig. 5(b)) managed to recover and reach a steady state. The level of channel flooding gradually decreases over time, while the steady state at 2.03 A cm^{-2} shows only minor water content (close to the outlet) at the end of the 40-min run. At lower flow rates (0.6 slpm air, Fig. 5(a)), the cell continued to operate with a partially flooded cathode flow field. Note that the fog coverage of the top plate may be misleading when estimating the level of channel flooding, as it is only the thin water layer accumulated on the top channel surface. Clear area in the last image in Fig. 5(a) at 40 min, does not necessarily mean that the level of channel flooding is lower than at 20 min. Rather, the fogged areas were cleared by and the water merged with the moving slugs from the upstream portion (two slugs in the clear areas of the third and fourth channel section from the bottom at 40 min are clearly visible).

At higher operating temperature of 70 °C (0.6/0.29 slpm, Fig. 5(c)), stepping down the voltage did not result in instantaneous flooding, seen through the absence of the steep decrease in the current draw after the initial jump. In addition, almost no liquid water was observed in the flow field. Further increase of the air flow rate to 1.1 slpm (at 70 °C) resulted in lower performance and higher current oscillations, suggesting that the cell was operating at the membrane dehydration limit.

3.2. Influence of the GDL material

Besides providing mechanical support for the MEA, the GDL serves to transport the reactants (electrons and humidified gases) to the catalyst layer, while removing the cathode reaction products (water and heat). As far as water management is concerned, the key role of the GDL media is to prevent excessive water accumulation in the catalyst layer, while keeping the membrane well hydrated. A detailed overview of the manufacturing processes, as well as characterization methods for the GDL materials is provided elsewhere [2]. Materials tested in our study represent three manufacturing techniques [2]: woven carbon fibers, i.e. cloth (AvCarb^{TM} 1071HCB by Ballard [16]), non-woven carbon paper (TGP-H-60 by Toray [17]), and non-woven, dry-laid fiber materials (by SGL Carbon [14,15]). The SGL materials are wet-proofed by 5 wt.% PTFE, in contrast to untreated carbon cloth and Toray paper (smooth, uncoated fibers in the last two SEM images, Fig. 2. In addition, SGL31BC and 35BC have a thin (20–30 μm) microporous layer (MPL) coated on the 5 wt.% PTFE carbon fiber substrate. MEAs with MPL had SGL31BA on the anode side, while the MPL was facing the cathode catalyst layer. Carbon fibers have approximately the same diameter for all materials tested, close to 8 μm. Toray paper and SGL carbon fiber materials (including the substrates for the MPL in 31BC and 35BC) have similar pore structure, with mean pore diameter (determined by capillary flow porometry) of 23 μm [2] and 31.4 μm [15], respectively. In contrast to the random pore structure of the aforementioned materials, carbon cloth has two-ply woven structure (Fig. 2), with transversely oriented top and bottom strands. Fibers within a strand form slit-shaped pores (typical pore width is on the order of the fiber diameter: 6–8 μm, with lengths up to 0.6 mm, i.e. along the entire exposed strand section).

Water management characteristics of different GDL materials were tested at the same operating conditions (Figs. 6 and 7). Wet-proofed SGL materials showed similar water dynamics as explained in the previous section, with droplets emerging at the surface over the entire visible area. Untreated GDLs did not exhibit such behavior. Instead of being expelled as discrete droplets from the pore openings, water tends to climb up the channel sidewall, and continue its movement along the serpentine mostly in the form of films and slugs clinging to the sidewall. This water removal mechanism is far less effective than the droplet egress/detachment, since it is narrowed down to the region of contact between the channel sidewalls and the GDL soaked with water.

The level of cathode flow field flooding was compared at similar current densities (i.e. similar water production rates). Images (a)–(d), Fig. 6, correspond to the enlarged symbols on the polarization curves (SGL31BA has been discussed earlier). Although the water production rate is about the same, there is hardly any visible liquid water when GDL is Toray paper (Fig. 6d). We conclude that the water has been trapped inside the GDL and the catalyst layer, hence the poor performance. Liquid water inside the flow field channels (when compared at same conditions and water production rate) means that excess water has been efficiently transported by the GDL away from the cathode. This tool can therefore be used to evaluate the water management capability of the GDL materials. Further, polarization curve slopes (Fig. 6) indicate significantly lower membrane ionic conductivity (i.e. hydration level) for the untreated GDLs. We infer that the poor membrane hydration is due to inability of the untreated GDLs to push the water to the membrane side through the catalyst layer, as they are also not able to efficiently expel the water into the flow channel.

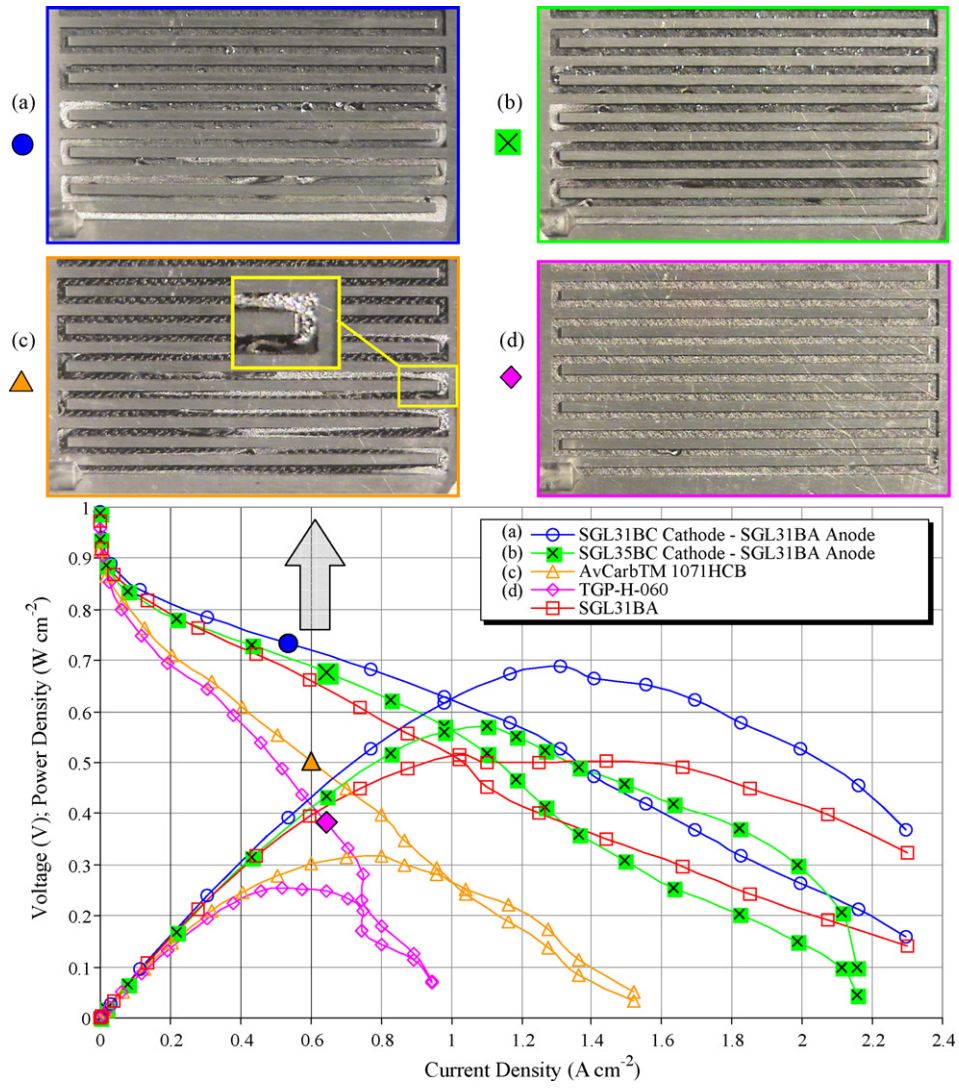

Fig. 6. Comparison of GDL materials at same operating conditions: 50 °C DPT/60 °C inlet/50 °C cell/(air/H_2) = (0.6/0.29 slpm). (a)–(d) Cathode flow field flooding compared at a similar current density.

Fig. 7 illustrates the ability of GDL media to reach steady state for mass transport after step changes in cell current draw. After the (much less pronounced) initial jump in the current draw, the untreated GDLs show a slowly decreasing trend in the current output. This can be explained by the fact that more GDL pores get saturated with water over time, thus preventing the access of the reactant gas to the catalyst layer. Again, only traces of liquid water in the channel were observed close to the cathode outlet for Toray paper (although at lower current density). Furthermore, this material is very sensitive to occasional bursts of liquid water from the testing installation (small drop in current at about 35 min after switching from OCV to 0.4 V). SGL materials continue to operate under flooded cathode flow field, accompanied by the increase in current as they recover from the initial flooding. Although having an MPL does not necessarily result in better performance, it has an interesting influence on water dynamics, observed through the increased water content on the anode side. As for the three GDLs without an MPL, we anticipated that higher cell performance was correlated with the higher in-plane permeability, due to the enhanced mass transport under the lands between the adjacent channels [20,21]. SGL31BA had the highest in-plane permeability, and TGP-H-60 the lowest [22].

3.3. Effect of the microporous layer

Microporous layer (MPL) was a mixture of carbon black and PTFE coated on the carbon fiber substrate with 5 wt.% PTFE [14,15]. In lower magnification SEM images (100×), the MPL surface appears smooth, with typical "mud cracks" (10–20 μm wide, 0.1–0.5 mm long) induced by the sintering step in the manufacturing process. Images taken at higher magnification (up to 10,000×) reveal the fine porous structure, with typical pore openings of 0.2–0.3 μm (Fig. 2). The mean (flow based) pore size of 4 μm was reported by the manufacturer [15], measured by the capillary flow porometry in a finished GDL product (i.e. with MPL already deposited on the fiber substrate).

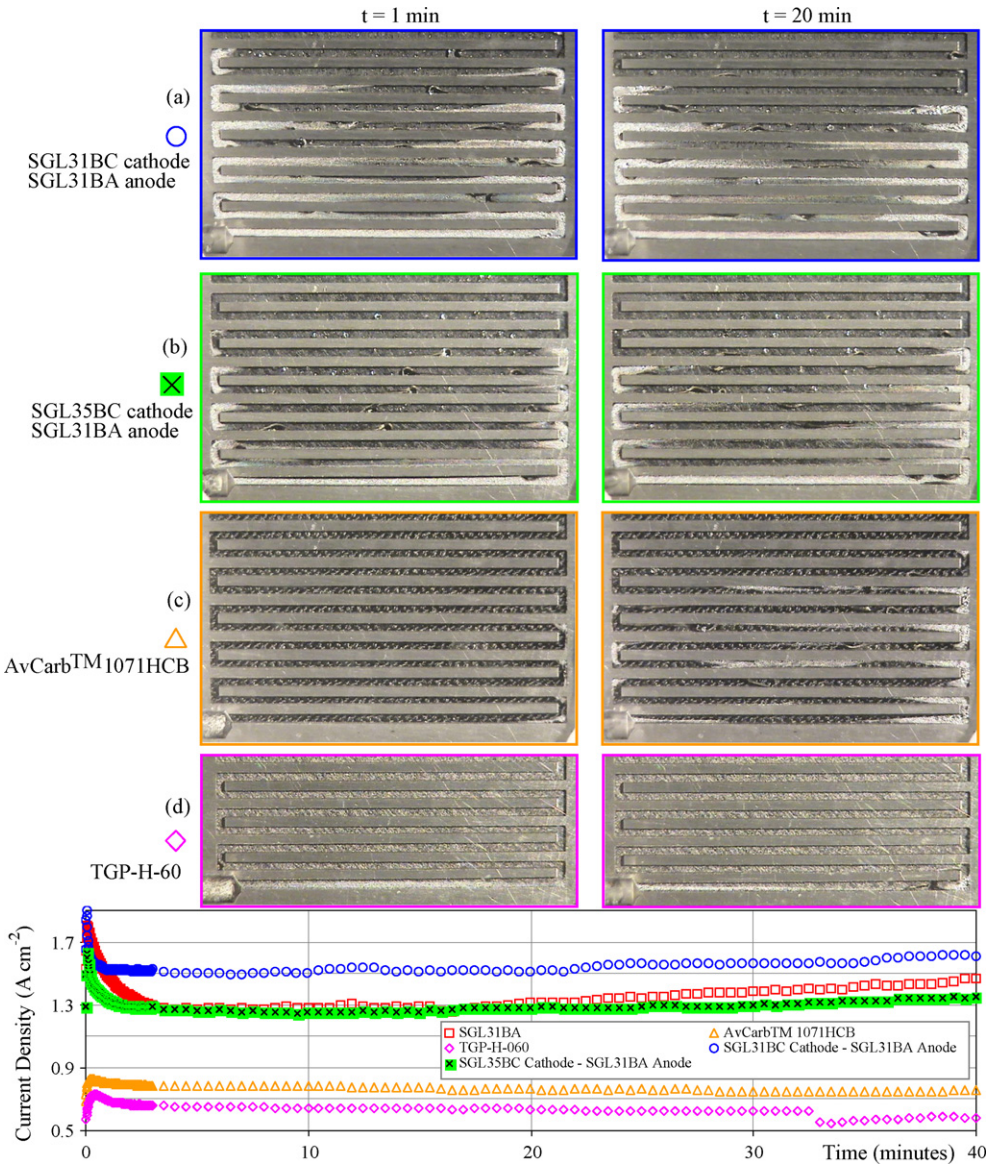

Fig. 7. Performance at constant voltage 0.4 V after OCV (same operating conditions as in Fig. 6).

Finally, we examined the influence of the microporous layer (structure shown in Fig. 2), by repeating the tests except that this time the anode side was visualized. No liquid water was observed in the anode flow field unless cathode GDLs had an MPL. MPL on the cathode side creates a pressure barrier for water produced at the catalyst layer. Water is pushed across the membrane to the anode side, resulting in anode flow field flooding and partial channel clogging close to the H_2 exit (Figs. 8 and 9). Liquid water in both the anode and cathode flow fields indicates that the membrane is well hydrated, which is one of the major benefits provided by the MPL (through increased membrane ionic conductivity). In addition, MPL provides more intimate contact with the catalyst layer, thus decreasing the electrical contact resistance. Adding an MPL can also reduce the difference in performance between different GDLs [13].

Liquid water buildup at the anode side (Fig. 8) was observed while recording the polarization curves (very similar to curves in Fig. 6). Unlike the cathode side, where droplets mainly emerge from the GDL pores, water on the anode side typically builds up from the channel walls as the unconsumed hydrogen reaches saturation before leaving the cell. Water accumulates at U-turns, originating mainly from the outer sidewalls of the bend. These locations of typical water buildup can be attributed to the corner flow effects of the main gas stream. After exceeding a current density of about 1.7 A cm^{-2}, water is evaporated yielding a dry anode flow field. This could be explained as follows. At higher current density, the effect of electro-osmotic drag is more pronounced, decreasing the net water transport to the anode side. Second (and probably more influential), the experimental cell was cooled by natural convection only, resulting in increased cell temperature at high current densities (55–57 °C at the limiting current, for cell heaters set at 50 °C).

The anode side was then visualized at constant currents (0.5, 1, and 1.5 A cm^{-2}) for 2 h, after switching from OCV (Fig. 9). There was no visible water in the flow field at OCV and 0.5 A cm^{-2}. Slightly more water was observed at 1 A cm^{-2}

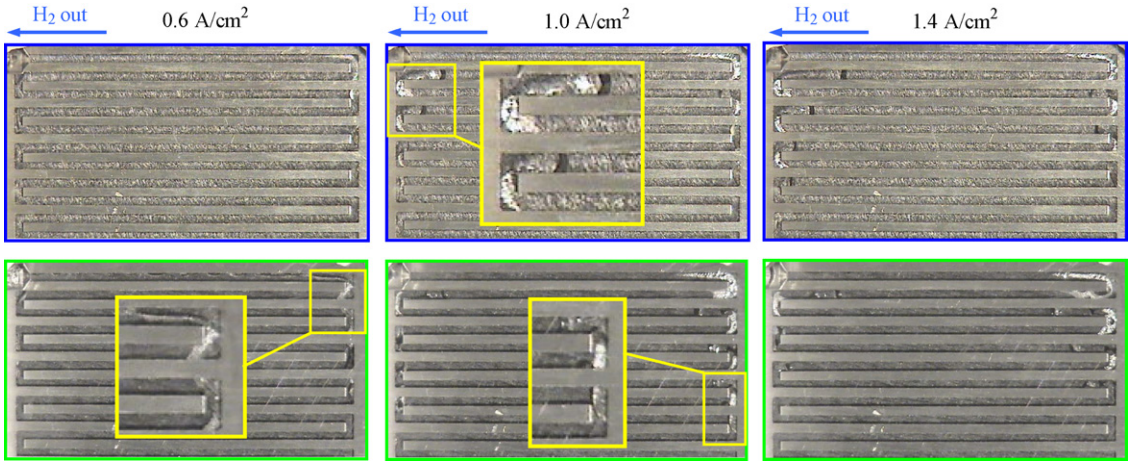

Fig. 8. Effect of MPL: anode flow field flooding (same operating conditions as in Fig. 6). Top row: SGL31BC cathode/SGL31BA anode; Bottom row: SGL35BC cathode/SGL31BA anode.

than at 1.5 A cm^{-2}, due to the increased cell temperature and electro-osmotic drag at higher current. The MPL effect was visible after less than 1 min, as water started to condense on the channel sidewall close to the outlet. Unlike the dynamic droplet movements observed on the cathode side, water is removed from the flow field mainly in vapor form.

Water condensation on the anode side was previously observed by neutron imaging [11]. Condensation occurred purely because of already saturated hydrogen feed (at very low flow rate), which was confirmed at open circuit conditions. In addition, GDLs employed in [11] did not have an MPL. However, no liquid water was observed in our experiments at open circuit (not even after running the cell at 0.5 A cm^{-2} for 2 h), whereas anode flow field flooding was obvious at higher current densities. We therefore conclude that water accumulation on the anode side was caused by water transport across the membrane, in addition to the water already carried into the cell by the humidified hydrogen feed. Clearly, this mechanism is competing with the electro-osmotic drag. To more carefully examine the influence of GDL/MPL materials on the net water transport across the membrane, water collection apparatus for both sides of the cell will be added in our future experiments.

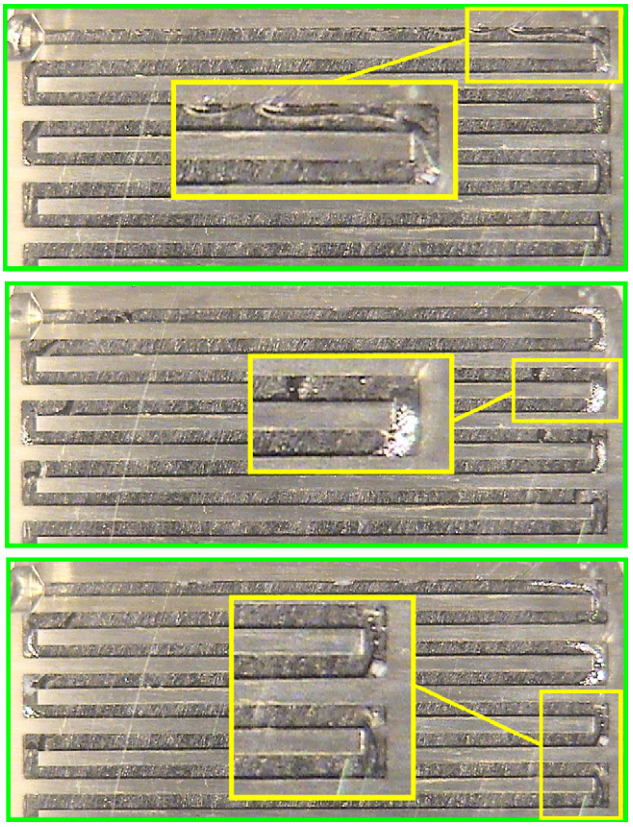

Fig. 9. Time evolution of the anode flow field flooding for SGL35BC cathode/SGL31BA anode at const 1.5 A cm^{-2} after switching from OCV. Top to bottom: 5 min (0.40 V); 10 min (0.41 V); 120 min (0.42 V).

There are several effects that the MPL has on the water dynamics. First, saturated vapor pressure is higher inside the MPL, because of the smaller pore size (Fig. 2) and increased hydrophobicity. Therefore, the MPL is less prone to flooding. This effect is commonly modeled by the Kelvin equation [4,5], although the validity of the equation might be questionable if the pores are too small. Second, it takes much higher pressure for the liquid water to break through the MPL pores. There is a subtle difference between the two effects, although both stem from the fact that the MPL pores are small and hydrophobic. A simple experiment was performed to illustrate the second effect: the water head was gradually increased in acrylic tubes (2.5 cm diameter) with their bottom ends covered by GDL samples until water started to flow through the pores. Samples with an MPL (SGL31BC and SGL35BC) could support a threshold water head of 75 cm compared with 15 cm of the SGL31BA. No such pressure barrier could be defined for the untreated GDLs, as water easily flowed in a continuous stream through the samples. Revisiting the discussion from the previous section, wet-proofed GDL acts as a pressure valve, with much higher burst pressure when the MPL is present. This barrier has a two-fold function: while pushing the water to the membrane side, it also provides a pressure buildup necessary to expel the water through the less hydrophobic GDL pores into the cathode channel. In order to achieve better performance through water management by the

MPL, we conclude that the MPL properties need to be tailored for specific CCM, cell design, and operating conditions. For example, membrane material and the catalyst layer need to be able to efficiently transport the water to the anode side. Further, if the MPL pressure barrier is too high, it might result in lower performance due to cathode catalyst flooding.

3.4. Two-phase flow: single-serpentine versus parallel flow field

For the range of the air flow rates from 0.6 to 1.3 slpm (50 °C, 1 bar backpressure), the inlet velocities and Reynolds numbers range from 7.4 m s^{-1} ($Re = 726$) to 16 m s^{-1} ($Re = 1572$), respectively for the single-serpentine channel. For the same air flow rate, Reynolds number is higher in the serpentine configuration, since the flow rate per cross section of a single channel is higher when compared to that of multiple parallel channels. Higher gas velocity and multiple U-turns make the two-phase transport more dynamic than in the parallel flow field. Further, when a parallel channel is blocked by liquid water, the air chooses a path of lesser resistance (through the remaining unblocked channels), thus leaving the blocked channel starved of the reactant gas [7,9]. The cell can continue to operate at significantly lower power output for extended periods due to the idle channel(s). On the other hand, only instantaneous serpentine channel blockage could be observed: air immediately either breaks through the blockage, or expels the accumulated water in the form of fast-moving slugs. In addition to evaporation and shear flow, another mechanism of water removal from the flow field is by collection of smaller stationary droplets by moving drops and slugs. Often a single detached droplet triggers the water movement in a large downstream portion. Large drops and fast-moving slugs coalesce with, and sweep away, stationary droplets attached to the GDL or the wall surface thereby enhancing water removal. This is a dynamic process, and the active cell area changes in response to water movement along the channel, causing temporal fluctuations in cell power, rather than a sharp extended drop encountered in the parallel configuration. Further, water removal from the GDL is helped by the convective portion of the air flow under the lands, due to pressure difference between adjacent serpentine channel sections [20–22]. Liquid water accumulation at U-turns is characteristic for the serpentine flow field, as a consequence of the corner flow effects of the main gas flow [19]. It would be worthwhile to mitigate water stagnation by hydrophobic treatment of the channel walls in these regions (especially the outer corners of the U-bend). Finally, it would be worthwhile to visualize the parallel anode flow field and check the influence of MPL on water management. We anticipate that prolonged anode channel blockage will occur under certain operating conditions, similar to that observed on the cathode side in previous parallel flow field studies [7,9].

4. Conclusions

Two-phase dynamics were investigated by experimental visualization for different GDL materials in a single-serpentine hydrogen-air PEMFC. The level of the cathode flow field flooding at specified current density and same operating conditions can be used as a criterion to evaluate the water management capability of the GDL materials. At similar current density (i.e. water production rate), lower water content in the cathode channel indicated that liquid water had been trapped inside the GDL pores and the catalyst layer, resulting in lower output voltage. Such behavior was typical for the untreated GDLs. From our experiments, poor cell performance with the untreated GDLs can be correlated with water management and summarized as follows: (1) Untreated GDLs were not able to push the water to the membrane side, which resulted in low ionic conductivity of the membrane (as indicated by the steep slope of the polarization curve). (2) Gas transport was inhibited by the pores saturated with liquid water. (3) Liquid water removal from the GDL into the flow channel was to a large extent limited to the narrow region of contact between the sidewalls and the GDL. In contrast, wet-proofed GDLs managed to expel water in the form of discrete droplets over the entire exposed GDL/channel interface, while leaving majority of the pores available for gas transport. In addition, high-velocity gas stream in the serpentine (from 7.4 m s^{-1}, with $Re = 726$) readily detached the emerging droplets from the GDL pores. Time evolution studies at fixed voltage showed a slowly increasing trend in current for the wet-proofed GDLs, having recovered from the initial flooding caused by the jump in water production rate. Single-serpentine cell was able to operate with high liquid water content in the flow field over time, attributed to the efficient water removal through the flow field, without prolonged channel blockage.

The pressure barrier, characteristic of the wet-proofed GDLs, was shown to be a crucial factor for the efficient water transport into the flow channel, and especially for membrane hydration. Adding an MPL to the wet-proofed substrate increases the pressure barrier five times, resulting in a well-hydrated membrane. This effect was observed through the anode flow field flooding close to the H_2 exit, as water was pushed across the membrane to the anode side when the current density of 0.5 A cm^{-2} was exceeded. We anticipate a competing effect between the membrane hydration via MPL and the extended blockage of the parallel anode channels.

Acknowledgements

We acknowledge funding for this research by the US Department of Energy grant DE-FG02-04ER63820, and Delaware Natural Resource and Environmental Control (DENREC) award No. 01040000450. The authors would like to thank Mr. Dan McCluskey of SGL Carbon Group for providing the GDL samples with MPL. We also thank Dr. Joseph Deitzel of the Center for Composite Materials at the University of Delaware, for his help with the high-speed camera.

References

[1] J. Larminie, A. Dicks, Fuel Cell Systems Explained, John Wiley & Sons LTD, 2001, Chapter 4.

[2] M. Mathias, J. Roth, J. Fleming, W. Lehner, in: W. Vielstich, A. Lamm, H.A. Gasteiger (Eds.), Handbook of Fuel Cells—Fundamentals, Technology and Application, vol. 3, Wiley, 2003, Chapter 46.
[3] W. He, G. Lin, T.V. Nguyen, AIChE J. 49 (12) (2003) 3221–3228.
[4] A.Z. Weber, R.M. Darling, J. Newman, J. Electrochem. Soc. 151 (10) (2004) 1715–1727.
[5] A.Z. Weber, R.M. Darling, J. Newman, J. Electrochem. Soc. 152 (4) (2005) 677–688.
[6] F. Barbir, H. Gorgun, X. Wang, J. Power Sources 141 (2005) 96–101.
[7] K. Tüber, D. Pócza, C. Hebling, J. Power Sources 124 (2003) 403–414.
[8] H. Hakenjos, U. Muenter, C. Wittstadt, Hebling, J. Power Sources 131 (2004) 213–216.
[9] X.G. Yang, F.Y. Zhang, A.L. Lubawy, C.Y. Wang, Electrochem. Solid State Lett. 7 (11) (2004) 408–411.
[10] F.Y. Zhang, X.G. Yang, C.Y. Wang, J. Electrochem. Soc. 153 (2) (2006) 225–232.
[11] N. Pekula, K. Heller, P.A. Chuang, A. Turhan, M.M. Mench, J.S. Brenizer, K. Ünlü, Nucl. Instrum. Methods Phys. Res., Sect. A 542 (2005) 134–141.
[12] S. Tsushima, K. Teranishi, S. Hirai, Electrochem. Solid State Lett. 7 (9) (2004) 269–272.
[13] Z. Qi, A. Kaufman, J. Power Sources 109 (2002) 38–46.
[14] http://www.sglcarbon.com.
[15] P.M. Wilde, M. Mandle, M. Murata, N. Berg, Fuel Cells 4 (3) (2004) 180–184.
[16] http://www.ballard.com/resources/carbon_fiber/BMP_AVCARB_FABRICS_10.04.pdf.
[17] http://www.torayca.com/index2.html.
[18] P. Concus, R. Finn, Proc. Natl. Acad. Sci. U.S.A. 63 (1969) 292–299.
[19] J. Martin, P. Oshkai, N. Djilali, ASME J. Fuel Cell Sci. Technol. 2 (2005) 70–80.
[20] J.P. Feser, A.K. Prasad, S.G. Advani, J. Power Sources 161 (2006) 404–412.
[21] M.V. Williams, H.R. Kunz, J.M. Fenton, J. Electrochem. Soc. 151 (10) (2004) 1617–1627.
[22] J.P. Feser, A.K. Prasad, S.G. Advani, J. Power Sources 162 (2006) 1226–1231.